Journal of Solid State Chemistry 182 (2009) 421–427

Contents lists available at ScienceDirect

Journal of Solid State Chemistry

journal homepage: www.elsevier.com/locate/jssc

Syntheses, structures and photoluminescence of a series of lanthanide-organic frameworks involving in situ ligand formation

Xiandong Zhu [a,b], Shuiying Gao [a], Yafeng Li [a], Hongxun Yang [a], Guoliang Li [a], Bo Xu [a], Rong Cao [a,*]

[a] State Key Laboratory of Structural Chemistry, Fujian Institute of Research on the Structure of Matter, Chinese Academy of Sciences, Fuzhou 350002, PR China
[b] Department of Biochemical Engineering, Anhui University of Technology and Science, Wuhu 241000, PR China

ARTICLE INFO

Article history:
Received 19 July 2008
Received in revised form
21 October 2008
Accepted 3 November 2008
Available online 21 November 2008

Keywords:
Lanthanide-organic frameworks
In situ reaction
Photoluminescence

ABSTRACT

A series of lanthanide-organic frameworks with aromatic pyridinecarboxylate ligand, generally formulated as $[Ln(PYDC)(C_2O_4)_{0.5}(H_2O)_2]\cdot H_2O$ (Ln = Pr(**1**), Nd(**2**), Eu(**3**), Gd(**4**), Tb(**5**), Er(**6**); H_2PYDC = 3,4-pyridinedicarboxylic acid) have been successfully synthesized and characterized. Their isostructures are built up from one-dimensional (1D) infinite chains cross-linked via the tri-connected PYDC ligands, leading to the two-dimensional (2D) layer structure. The adjacent layers are further extended into three-dimensional (3D) supramolecular frameworks through hydrogen bonding and π–π stacking interactions. Interestingly, the oxalate bridging ligand is believed to form via in situ ligand synthesis through decarboxylation of the organic precursor, H_2PYDC. Complexes **3** and **5** exhibit strong fluorescent emissions in the visible region at room temperature.

1. Introduction

Luminescent lanthanide-organic frameworks are currently of great interest and importance, not only because of their fascinating architectures but also owing to their technological importance, such as diagnostic tools, luminescent sensors, laser systems, and optical amplification for telecommunications [1–4]. The trivalent lanthanide ions are very attractive luminescent centers for their high color purities and relatively long lifetimes of the excited states as a result of transitions within the partially filled 4*f* shell of the ions. Complexes of Eu^{3+} and Tb^{3+} showing strong luminescence in the visible region have been widely exploited in applications such as fluoroimmunoassays and structural probes [5–7]. More recently, there has been increasing interest in the design of complexes with lanthanide ions that show emissions in the near-infrared region (800–1550 nm), such as Nd^{3+}, Yb^{3+}, and Er^{3+} for their potential use in luminescent bioassays, laser systems and optical amplification [8–11]. Since the weak absorption coefficient of the parity-forbidden transitions, luminescence from lanthanide ions is usually sensitized by suitable organic chromophores [12–14]. This "antenna effect" involves energy transfer from excited π molecular orbital of conjugated ligands to the lanthanide centers. Through the elaborate choice of multifunctional organic linkers and effective synthetic strategy, lanthanide-organic frameworks exhibiting intense and long-lived fluorescent emissions could be achieved [15–18]. Unsymmetrical 3,4-pyridinedicarboxylic acid (H_2PYDC), possessing electron-conjugate systems and multiple binding sites, may be good chromophore candidates for the efficient luminescent sensitization of lanthanide ions. On the other hand, hydro(solvo)thermal in situ metal/ligand reactions is of great interest in coordination chemistry and organic chemistry due to its effectiveness, simplicity and environmental friendliness [19,20]. A variety of novel coordination complexes synthesized in situ have been documented and many type of in situ reactions have been observed in hydrothermal systems [21–26]. Under these conditions, the in situ formation of organic species often relies on the rearrangement or cleavage of original ligand. Herein, we present the systematic investigation of the syntheses, crystal structures and photoluminescencent properties of a series of lanthanide-organic frameworks with aromatic pyridinecarboxylate ligand, generally formulated as $[Ln(PYDC)(C_2O_4)_{0.5}(H_2O)_2]\cdot H_2O$ (Ln = Pr(**1**), Nd(**2**), Eu(**3**), Gd(**4**), Tb(**5**), Er(**6**)). Interestingly, the oxalate bridging ligand is believed to form via in situ ligand synthesis through decarboxylation of the organic precursor, H_2PYDC.

2. Experimental section

2.1. Materials and general methods

All commercially available reagents and starting materials were of reagent-grade quality and used without further purification. Elemental analyses (C, H, N) were carried out on an

* Corresponding author. Fax: +86 591 83796710.
E-mail address: rcao@fjirsm.ac.cn (R. Cao).

0022-4596/$ - see front matter © 2008 Elsevier Inc. All rights reserved.
doi:10.1016/j.jssc.2008.11.012

Elementar Vario EL III analyzer. Infrared (IR) spectra were recorded on PerkinElmer Spectrum One as KBr pellets in the range 4000–400 cm^{-1}. Thermogravimetric analysis was recorded with a NETZSCH STA 449C unit at a heating rate of 10 °C min^{-1} under nitrogen atmosphere. Solid-state luminescence spectra in the visible range were measured at room temperature with an Edinburgh Instrument FLS920 fluorescence spectrometer. This instrument is equipped with an Edinburgh Xe900 xenon arc lamp as exciting light source.

2.2. Syntheses of the compounds

2.2.1. Synthesis of $[Pr(PYDC)(C_2O_4)_{0.5}(H_2O)_2]\cdot H_2O$ (**1**)

A mixture of Pr_6O_{11} (0.031 g, 0.03 mmol) and H_2PYDC (0.034 g, 0.20 mmol) in deionized water (10 mL) was adjusted to pH = 2.5 with 2 mol/L HNO_3, sealed in a 25 mL Teflon-lined stainless steel autoclave, and heated at 180 °C for 72 hours, then slowly cooled to room temperature during 24 hours. Prismatic crystals were recovered by filtration, washed by distilled water, and dried in air at ambient temperature. Yield: 56% (based on H_2PYDC). Calcd for $C_8H_9PrNO_9$ (404.07): C 23.78, H 2.25, N 3.47; found: C 23.38, H 2.41, N 3.25. IR (KBr, cm^{-1}): 3435 (s, br), 1658 (s), 1613 (m), 1562 (vs), 1489 (m), 1432 (s), 1393 (m), 1312 (w), 1162 (w), 1125 (w), 1050 (w), 849 (w), 820 (w), 727 (w), 682 (w).

2.2.2. Synthesis of $[Nd(PYDC)(C_2O_4)_{0.5}(H_2O)_2]\cdot H_2O$ (**2**)

Compound **2** was prepared in the same way as that for **1** but using Nd_2O_3 (0.034 g, 0.10 mmol) and H_2PYDC (0.034 g, 0.20 mmol) as the reactants. Yield: 49% (based on H_2PYDC). Calcd for $C_8H_9NdNO_9$ (407.40): C 23.59, H 2.23, N 3.44; found: C 23.19, H 2.47, N 3.32. IR (KBr, cm^{-1}): 3442 (s, br), 1657 (s), 1615 (m), 1564 (vs), 1490 (m), 1432 (s), 1394 (m), 1313 (w), 1163 (w), 1128 (w), 1052 (w), 850 (w), 820 (w), 728 (w), 680 (w).

2.2.3. Synthesis of $[Eu(PYDC)(C_2O_4)_{0.5}(H_2O)_2]\cdot H_2O$ (**3**)

Compound **3** was prepared in the same way as that for **1** but using Eu_2O_3 (0.035 g, 0.10 mmol) and H_2PYDC (0.034 g, 0.20 mmol) as the reactants. Yield: 63% (based on H_2PYDC). Calcd for $C_8H_9EuNO_9$ (415.12): C 23.15, H 2.19, N 3.37; found: C 22.89, H 2.55, N 3.46. IR (KBr, cm^{-1}): 3446 (s, br), 1665 (s), 1615 (m), 1566 (vs), 1493 (m), 1435 (s), 1394 (m), 1315 (w), 1163 (w), 1127 (w), 1059 (w), 852 (w), 820 (w), 729 (w), 683 (w).

2.2.4. Synthesis of $[Gd(PYDC)(C_2O_4)_{0.5}(H_2O)_2]\cdot H_2O$ (**4**)

Compound **4** was prepared in the same way as that for **1** but using Gd_2O_3 (0.036 g, 0.10 mmol) and H_2PYDC (0.034 g, 0.20 mmol) as the reactants. Yield: 45% (based on H_2PYDC). Calcd for $C_8H_9GdNO_9$ (420.41): C 22.86, H 2.16, N 3.33; found: C 22.52, H 2.74, N 2.98. IR (KBr, cm^{-1}): 3434 (s, br), 1669 (s), 1614 (m), 1565 (vs), 1492 (m), 1435 (s), 1393 (m), 1316(w), 1163 (w), 1127 (w), 1058 (w), 856 (w), 820 (w), 730 (w), 683 (w).

2.2.5. Synthesis of $[Tb(PYDC)(C_2O_4)_{0.5}(H_2O)_2]\cdot H_2O$ (**5**)

Compound **5** was prepared in the same way as that for **1** but using Tb_2O_3 (0.037 g, 0.10 mmol) and H_2PYDC (0.034 g, 0.20 mmol) as the reactants. Yield: 66% (based on H_2PYDC). Calcd for $C_8H_9TbNO_9$ (422.08): C 22.76, H 2.15, N 3.32; found: C 22.35, H 2.61, N 3.26. IR (KBr, cm^{-1}): 3410 (s, br), 1672 (s), 1613 (m), 1567 (vs), 1492 (m), 1435 (s), 1393 (m), 1317 (w), 1163 (w), 1127 (w), 1058 (w), 858 (w), 819 (w), 730 (w), 683 (w).

2.2.6. Synthesis of $[Er(PYDC)(C_2O_4)_{0.5}(H_2O)_2]\cdot H_2O$ (**6**)

Compound **6** was prepared in the same way as that for **1** but using Er_2O_3 (0.038 g, 0.10 mmol) and H_2PYDC (0.034 g, 0.20 mmol) as the reactants. Yield: 52% (based on H_2PYDC). Calcd for $C_8H_9ErNO_9$ (430.42): C 22.32, H 2.11, N 3.25; found: C 22.05, H 2.78, N 3.22. IR (KBr, cm^{-1}): 3423 (s, br), 1669 (s), 1613 (m), 1566 (vs), 1492 (m), 1437 (s), 1394 (m), 1316(w), 1164 (w), 1125 (w), 1058 (w), 856 (w), 820 (w), 729 (w), 683 (w).

2.3. X-ray crystallographic study

Data collection was performed on a Rigaku Mercury CCD diffractometer with graphite-monochromated Mo*K*α ($\lambda = 0.71073$ Å) radiation at room temperature. All absorption corrections were performed by using the *CrystalClear* program [27]. The structures were solved by direct methods and refined by the full-matrix least-squares on F^2 using the *SHELXTL*-97 program [28]. All non-hydrogen atoms were treated anisotropically. The positions of hydrogen atoms attached to carbon atoms were generated geometrically (C–H bond fixed at 0.95 Å). Idealized positions of

Table 1
Crystallographic data for complexes **1–6**.

	1	2	3	4	5	6
Empirical formula	$C_8H_9PrNO_9$	$C_8H_9NdNO_9$	$C_8H_9EuNO_9$	$C_8H_9GdNO_9$	$C_8H_9TbNO_9$	$C_8H_9ErNO_9$
Formula weight	404.07	407.40	415.12	420.41	422.08	430.42
Crystal system	Triclinic	Triclinic	Triclinic	Triclinic	Triclinic	Triclinic
Space group	*P*−1	*P*−1	*P*−1	*P*−1	*P*−1	*P*−1
a (Å)	6.066(3)	6.1157(2)	6.070(2)	6.0592(19)	6.031(3)	5.9693(15)
b (Å)	10.156(5)	10.2888(4)	10.163(4)	10.135(3)	10.109(5)	10.131(3)
c (Å)	11.311(6)	11.446	11.329(4)	11.304(4)	11.256(5)	11.165(3)
α (deg)	105.86(2)	106.92(2)	105.68(2)	105.61(2)	105.10(3)	104.157(16)
β (deg)	101.018(18)	101.508(19)	100.937(15)	100.855(17)	100.465(19)	99.811(12)
γ (deg)	105.12(2)	104.859(16)	105.132(14)	105.169(15)	105.297(19)	105.314(10)
V ($Å^3$)	620.7(5)	636.05(3)	623.5(4)	619.8(3)	615.6(5)	611.2(3)
Z	2	2	2	2	2	2
ρ_{calc} (g/cm^3)	2.162	2.127	2.211	2.253	2.277	2.339
μ (mm^{-1})	3.966	4.122	5.071	5.392	5.787	6.908
*R*1,[a] w*R*2[b] ($I>2\sigma(I)$)	0.0336, 0.0915	0.0272, 0.0731	0.0302, 0.0819	0.0293, 0.0775	0.0340, 0.0941	0.0396, 0.1044
*R*1,[a] w*R*2[b] (all data)	0.0358, 0.0933	0.0297, 0.0751	0.0333, 0.0840	0.0317, 0.0790	0.0370, 0.0956	0.0426, 0.1058
GOF on F^2	1.045	1.088	1.055	1.060	1.073	1.049

[a] $R = \Sigma||Fo|-|Fc||/\Sigma|Fo|$.
[b] $wR(F^2) = [\Sigma w(Fo^2-Fc^2)^2/\Sigma w(Fo^2)^2]^{1/2}$.

Table 2
Selected bond lengths (Å) for complex **1–6**.

Compound 1[a]			
Pr(1)–O(1)	2.459(4)	Pr(1)–O(5)	2.448(4)
Pr(1)–O(2)#1	2.414(4)	Pr(1)–O(6)#2	2.427(4)
Pr(1)–O(3)#3	2.449(3)	Pr(1)–O(1W)	2.393(4)
Pr(1)–O(4)#3	2.489(4)	Pr(1)–O(2W)	2.375(4)
Pr(1)–O(2)	2.723(4)		
Compound 2[b]			
Nd(1)–O(1)	2.537(3)	Nd(1)–O(5)	2.487(3)
Nd(1)–O(2)	2.498(3)	Nd(1)–O(6)#2	2.469(3)
Nd(1)–O(3)#3	2.519(3)	Nd(1)–O(1W)	2.446(3)
Nd(1)–O(4)#1	2.466(3)	Nd(1)–O(2W)	2.415(3)
Nd(1)–O(4)#3	2.699(3)		
Compound 3[c]			
Eu(1)–O(1)	2.494(4)	Eu(1)–O(5)	2.433(4)
Eu(1)–O(2)	2.453(3)	Eu(1)–O(6)#2	2.453(4)
Eu(1)–O(3)#3	2.464(4)	Eu(1)–O(1W)	2.383(4)
Eu(1)–O(4)#1	2.413(4)	Eu(1)–O(2W)	2.369(5)
Eu(1)–O(4)#3	2.725(4)		
Compound 4[d]			
Gd(1)–O(1)	2.446(3)	Gd(1)–O(5)	2.423(4)
Gd(1)–O(2)	2.486(4)	Gd(1)–O(6)#2	2.442(4)
Gd(1)–O(3)#1	2.397(4)	Gd(1)–O(1W)	2.364(4)
Gd(1)–O(4)#3	2.449(4)	Gd(1)–O(2W)	2.379(4)
Gd(1)–O(3)#3	2.740(4)		
Compound 5[e]			
Tb(1)–O(1)	2.366(4)	Tb(1)–O(5)	2.433(4)
Tb(1)–O(2)#2	2.420(4)	Tb(1)–O(6)#1	2.395(4)
Tb(1)–O(3)#3	2.427(4)	Tb(1)–O(1W)	2.349(4)
Tb(1)–O(4)#3	2.467(4)	Tb(1)–O(2W)	2.360(4)
Tb(1)–O(1)#2	2.789(5)		
Compound 6[f]			
Er(1)–O(1)	2.441(5)	Er(1)–O(5)	2.362(5)
Er(1)–O(2)	2.391(5)	Er(1)–O(6)#3	2.409(5)
Er(1)–O(3)#2	2.370(5)	Er(1)–O(1W)	2.331(5)
Er(1)–O(4)#1	2.301(5)	Er(1)–O(2W)	2.318(6)
Er(1)–O(4)#2	2.976(4)		

Symmetry transformations used to generate equivalent atoms: [a](#1) $-x+1, -y, -z$; (#2) $-x+2, -y+1, -z$; (#3) $-x+2, -y, -z$. [b](#1) $x+1, y, z$; (#2) $-x+1, -y, -z$; (#3) $-x+1, -y+1, -z$. [c](#1) $x-1, y, z$; (#2) $-x+1, -y+2, -z+1$; (#3) $-x+1, -y+1, -z+1$. [d](#1) $x-1, y, z$; (#2) $-x+2, -y+1, -z+2$; (#3) $-x+2, -y, -z+2$. [e](#1) $-x-1, -y, -z$; (#2) $-x, -y+1, -z$; (#3) $x-1, y, z$. [f](#1) $x-1, y, z$; (#2) $-x+1, -y, -z+2$; (#3) $-x+1, -y+1, -z+2$.

hydrogen atoms of water molecules were located from Fourier difference maps and refined isotropically. Crystallographic data and structure determination summaries are listed in Table 1. Selected bond lengths for complex **1–6** are listed in Table 2. CCDC-668577 (**1**), 668579 (**2**), 668575 (**3**), 668576 (**4**), 668580 (**5**), 668578 (**6**) contain the supplementary crystallographic data for this paper. Copies of these data can be obtained free of charge from The Cambridge Crystallographic Data Centre via www.ccdc.cam.ac.uk/data_request/cif.

3. Results and discussion

3.1. Crystal structural descriptions

Prismatic crystals of **1–6** have been successfully synthesized through the preheating and cooling-down crystallization approach. Single-crystal X-ray diffraction, elemental analysis, and vibrational spectroscopic studies preformed on complexes **1–6** reveal that they are isomorphous. Therefore, the structure of complex **3** is selected and described in detail to represent their frameworks.

X-ray diffraction study of complex **3** reveals that the asymmetric unit contains one crystallographically unique Eu(III) motif. As shown in Fig. 1, the Eu(III) atom is nine-coordinated by three pairs of chelating oxygen atoms from two different PYDC ligands and one oxalate unit, one bridging oxygen atoms from a carboxylate group of PYDC ligand, and two terminal oxygen atoms from water molecules. The resulting polyhedron of the Eu(III) coordination sphere is best described as a distorted tricapped trigonal prism. The Eu–O (carboxylate) bond distances range from 2.413(4) to 2.725(4) Å, and those of the Eu–O (aqua) bonds range from 2.369(5) to 2.383(4) Å, all of which are comparable to those reported for other europium–oxygen donor complexes [29,30]. A little longer Eu(1)–O(4A) bond distance of 2.725(4) Å than the others within the range 2.369(5)–2.494(4) Å can be considered as weaker interactions (Table 2). This represents bridging tridentate binding modes of the ligand (Scheme 1), in which the carboxylate group chelate to the metal center in addition to an adjacent metal atom [31]. It can also distinguish bridging tridentate from bridging bidentate binding modes by comparing the Ln–O bond distances of the other reported lanthanide complexes with PYDC ligand [31–33]. Thus, each PYDC ligand connects three Eu(III) atoms with its two carboxylate groups adopting bis(chelate)-monodentate coordination modes. It should be mentioned that the organic linkers coordinate to metal centers just using pendant carboxylate groups, whereas the nitrogen atoms are free of coordination.

In the polymeric structure of complex **3**, two crystallographically equivalent Eu(III) atoms are bridged by two carboxylate oxygen atoms from different ligands to give a binuclear unit with the Eu···Eu distance of 4.349 Å. All the binuclear units are connected together by oxalate linkers leading to one-dimensional (1D) infinite chains. The 1D infinite chains are further cross-linked via the tri-connected PYDC ligands, leading to the formation of the extended two-dimensional (2D) layer structure, as illustrated in Fig. 2. The adjacent layers are further extended into three-dimensional (3D) supramolecular frameworks through hydrogen bonding interactions among the carbon atoms and the aqua ligands [C(4)···O(2W), 2.673 Å]. In addition, π–π stacking interactions between the pyridine rings from adjacent layers with the interplanar distance of ca. 3.27 Å stabilize the structure further (Fig. 3).

3.2. Synthesis chemistry and formation of the oxalate ligand

It is interesting to note that the presence of oxalate ligand in the final product despite the fact that there was no oxalate acid introduced to the starting materials. To confirm the formation of oxalates, similar reactions were carried out. When we performed the reaction in the presence of sodium oxalate as a direct source of $C_2O_4^{2-}$, the same products could also be obtained and given higher yields. In addition, attempts to use other lanthanide oxides to synthesize analogous species have successfully produced a series of isomorphous substances when we firstly yield the products of complex **3**. Recently, the lanthanide-mediated in situ transformation of CO_2 to oxalate ligand under hydrothermal conditions has been observed [34–38]. Although the reaction mechanism is unclear, we supposed that oxalate might be derived from in situ decarboxylation of H_2PYDC and followed by coupling of CO_2 to produce the oxalate linkage [39–41]. Although the release of carboxylate groups of pyridinecarboxylates has been reported by several laboratories [42–45], the formation of oxalate from

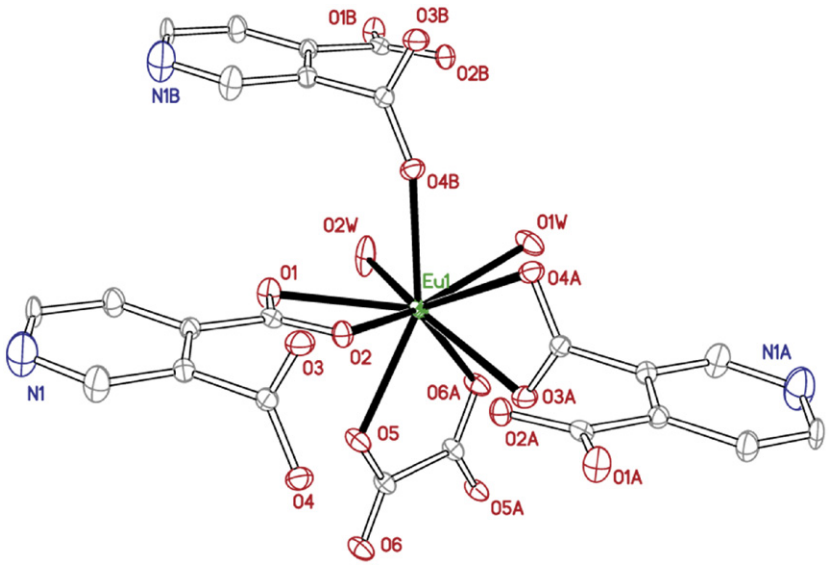

Fig. 1. ORTEP representation of the coordination environment of the nine-coordinated Eu(III) motif in complex **3**, with the thermal ellipsoids at 30% probability level.

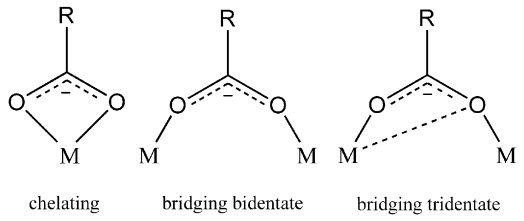

Scheme 1. Several different binding modes of carboxylate ligand discussed in the text.

pyridinecarboxylate ligand under hydrothermal conditions has been relatively less investigated [40].

3.3. Vibrational spectroscopic study

The analogous FT-IR spectra of complexes **1–6** are consistent with the structure analysis. The spectrum of complex **3** clearly exhibits the characteristic vibrational bands for carboxylate groups ($COO^{-}\cdots Ln^{3+}$) at 1566 cm^{-1} for the asymmetric stretching and at 1435 cm^{-1} for symmetric stretching. Meanwhile, the absence of the band ranging from 1690 to 1730 cm^{-1} ($\upsilon_{C=O}$ for COOH) demonstrates the complete deprotonation of the carboxylate groups. The strong and broad absorption centered at 3446 cm^{-1} is attributed to the presence of water molecules in the compound.

3.4. Photoluminescent properties

Taking into account the excellent luminescent properties of Eu(III) and Tb(III) ions in the visible region, the luminescent properties of complexes **3** and **5** were investigated in the solid state at room temperature. Complex **3** exhibits an intense, characteristic red europium emission upon excitation with a wavelength of 318 nm. As shown in Fig. 4, transitions from the excited $^5D_0$ state to the different *J*-levels of the lower ^7F state were observed in the emission spectrum ($J = 0$–2, 4), i.e., $^5D_0 \rightarrow {}^7F_0$ at 580 nm, $^5D_0 \rightarrow {}^7F_1$ at 593 nm, $^5D_0 \rightarrow {}^7F_2$ at 617 nm, and $^5D_0 \rightarrow {}^7F_4$ at 697 nm. It is well-known that the transition $^5D_0 \rightarrow {}^7F_0$ is strictly forbidden in a field of high symmetry and, therefore, the Eu(III) ions in complex **3** should occupy sites with low symmetry and no inversion center should be present for these sites, in agreement with the crystal structural analysis. The emission intensity of the so-called hypersensitive $^5D_0 \rightarrow {}^7F_2$ transition induced by electric dipole moment is five times compared to $^5D_0 \rightarrow {}^7F_1$ transition, which also demonstrates a lower symmetric coordination environment of the Eu(III) ions in the structure. Complex **5** gave typical terbium emission spectrum containing the expected sequence of $^5D_4 \rightarrow {}^7F_J$ ($J = 3$–6) transitions upon excitation at 318 nm (Fig. 5). The spectrum is dominated by the $^5D_4 \rightarrow {}^7F_5$ transition at 543 nm, which gave an intense green luminescence output for the sample. The other three bands at 490, 583, and 622 nm correspond to transition from $^5D_4$ state to $^7F_6$, $^7F_4$ and $^7F_3$ levels, respectively.

The luminescent decay curves of complexes **3** and **5** were obtained at room temperature. The decay curves are well fitted into a single-exponential function as $I = I_0 \exp(-t/\tau)$, indicating the occupation of the same average local environment of *Ln*(III) sites in the structure [46,47]. The corresponding lifetime for complex **3** is about 0.31 ms, whereas that for complex **5** is about 0.74 ms (determined by monitoring $^5D_0 \rightarrow {}^7F_2$ and $^5D_4 \rightarrow {}^7F_5$ line, respectively). Both of them have long luminescence lifetimes at millisecond order, which are comparable to other corresponding Eu(III) and Tb(III) complexes [48,49]. With respect to the free ligand, the strongest emission peak for H_2PYDC locates at ca. 370 nm ($\lambda_{ex} = 276$ nm) [50,51]. The absence of the ligand-centered emission in the fluorescence spectra for complexes **3** and **5**, suggests that the energy transfer from the ligand to the lanthanide center is efficient. Furthermore, the excitation spectra of **3** and **5** shows that the effective energy absorption mainly takes place in the region 250–350 nm (Fig. 6), which matches the absorption spectrum of the ligand; therefore, the ligand–lanthanide ions energy transfer is confirmed.

4. Conclusions

In summary, a series of lanthanide-organic frameworks with aromatic pyridinecarboxylate ligand, generally formulated as $[Ln(PYDC)(C_2O_4)_{0.5}(H_2O)_2]\cdot H_2O$ (*Ln* = Pr(**1**), Nd(**2**), Eu(**3**), Gd(**4**),

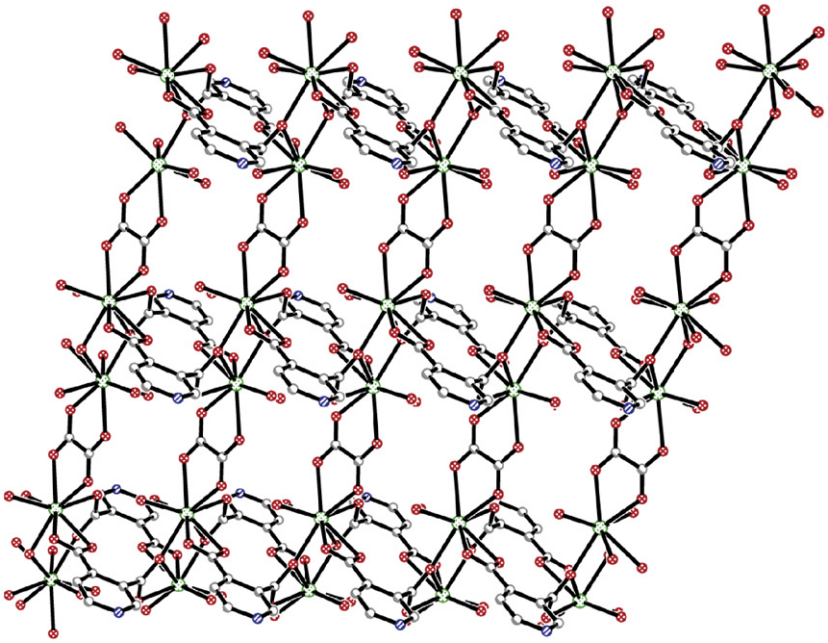

Fig. 2. View of two-dimensional framework of complex **3** constructed from one-dimensional infinite chains cross-linked via the tri-connected PYDC ligands.

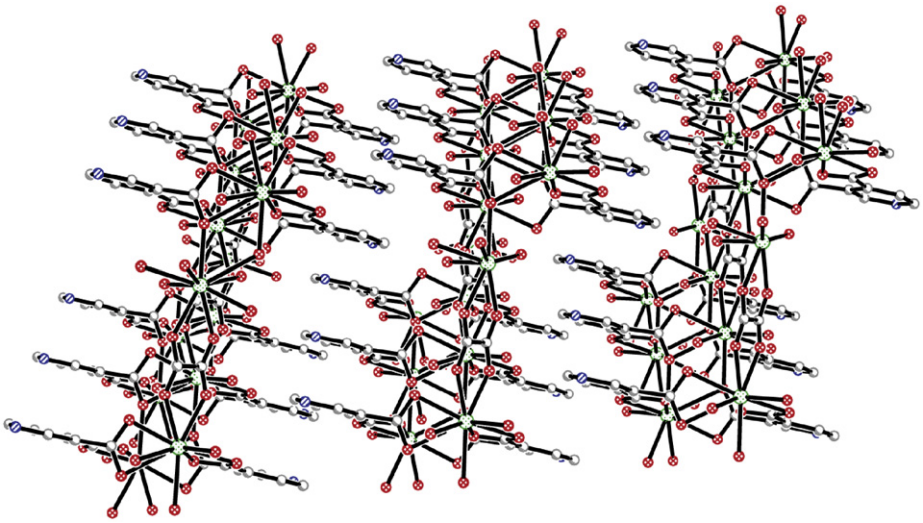

Fig. 3. Perspective view of three-dimensional supramolecular framework of complex **3** through hydrogen bonding and π–π stacking interactions.

Tb(**5**), Er(**6**)) have been successfully synthesized through the preheating and cooling-down crystallization approach. Their isostructures are built up from 1D infinite chains cross-linked via the tri-connected PYDC ligands, leading to the 2D layer structure. The adjacent layers are further extended into 3D supramolecular frameworks through hydrogen bonding and π–π stacking interactions. Interestingly, the oxalate bridging ligand is believed to form via in situ ligand synthesis through decarboxylation of the organic precursor, H_2PYDC. Complexes **3** and **5** exhibit strong fluorescent emissions in the visible region at room temperature. The energy transfer from the ligand to the lanthanide center is efficient. Thus, these complexes could be anticipated as good candidates for efficient luminescent materials and fluorescent probes.

Acknowledgments

This work was financially supported from 973 Program (2006CB932900/03), NSFC (20731005, 20521101, 20873151), NSF of Fujian Province (2006F3134, E0520003), Fujian Key Laboratory of Nanomaterials (2006L2005), "The Distinguished Oversea Scholar Project" and Key Project from CAS.

Appendix A. Supplementary data

Supplementary data associated with this article can be found in the online version at doi:10.1016/j.jssc.2008.11.012.

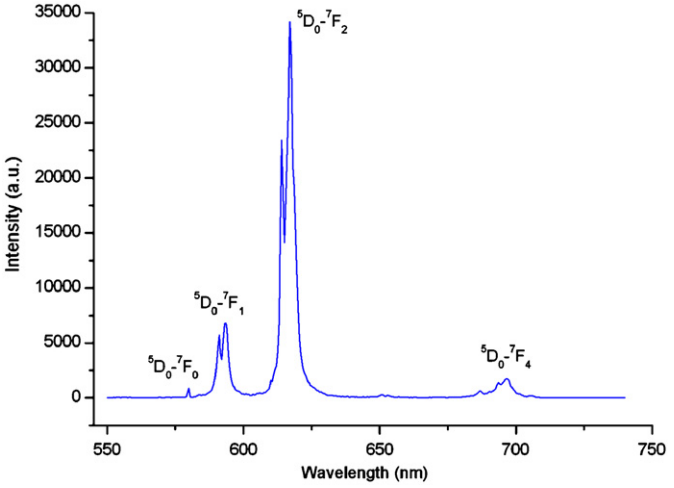

Fig. 4. Solid-state emission spectrum for complex **3** ($\lambda_{ex} = 318$ nm) at room temperature.

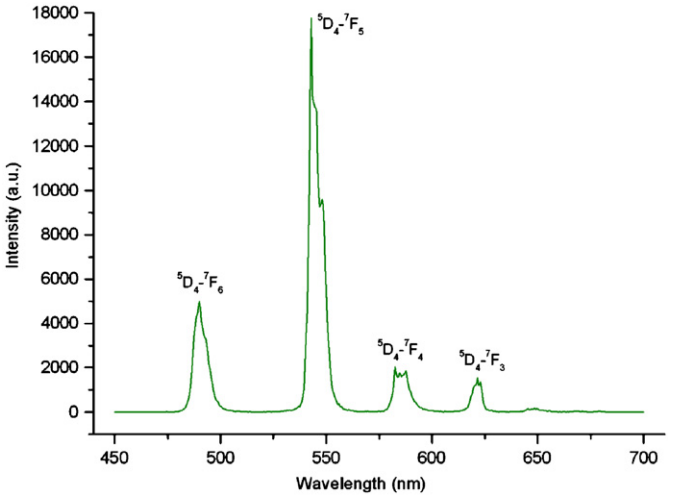

Fig. 5. Solid-state emission spectrum for complex **5** ($\lambda_{ex} = 318$ nm) at room temperature.

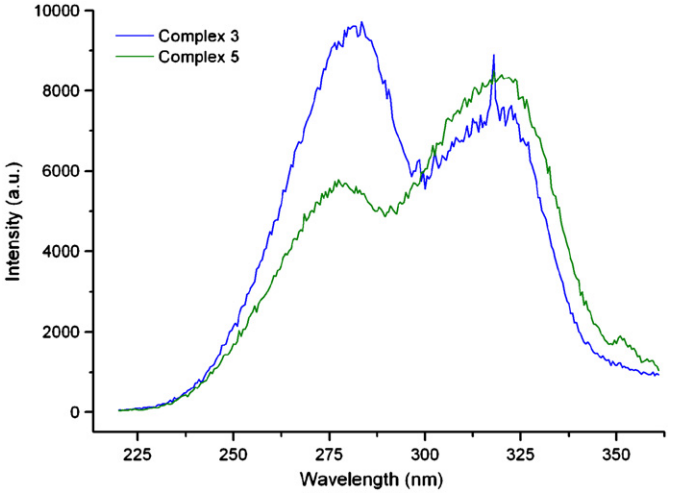

Fig. 6. Solid-state excitation spectra for complexes **3** and **5** at room temperature (monitored at 617 and 543 nm, respectively).

Appendix A. Supplementary data

References

[1] D. Parker, Coord. Chem. Rev. 205 (2000) 109.
[2] J. Kido, Y. Okamoto, Chem. Rev. 102 (2002) 2357.
[3] C. Benelli, D. Gatteschi, Chem. Rev. 102 (2002) 2369.
[4] G. Adachi, N. Imanaka, S. Tamura, Chem. Rev. 102 (2002) 2405.
[5] V.W.W. Yam, K.K.W. Lo, Coord. Chem. Rev. 184 (1998) 157.
[6] M. Montalti, L. Prodi, N. Zaccheroni, L. Charbonniere, L. Douce, R. Ziessel, J. Am. Chem. Soc. 123 (2001) 12694.
[7] D. Parker, R.S. Dickins, H. Puschmann, C. Crossland, J.A.K. Howard, Chem. Rev. 102 (2002) 1977.
[8] M.H.V. Werts, J.W. Hofstraat, F.A.J. Geurts, J.W. Verhoeven, Chem. Phys. Lett. 276 (1997) 196.
[9] Y. Hasegawa, T. Ohktbo, K. Sogabe, Y. Kawamura, Y. Wada, H. Nakashima, S. Yanagida, Angew. Chem. Int. Ed. 39 (2000) 357.
[10] K. Driesen, R.V. Deun, R.C. Görller-Walrand, K. Binnemans, Chem. Mater. 16 (2004) 1531.
[11] M.D. Ward, Coord. Chem. Rev. 251 (2007) 1663.
[12] M.H.V. Werts, M.A. Duin, J.W. Hofstraat, J.W. Verhoeven, Chem. Commun. (1999) 799.
[13] C. Yang, L.-M. Fu, Y. Wang, J.-P. Zhang, W.-T. Wong, X.-C. Ai, Y.-F. Qiao, B.-S. Zou, L.-L. Gui, Angew. Chem. Int. Ed. 43 (2004) 5010.
[14] R.V. Deun, P. Nockemann, P. Fias, K.V. Hecke, L.V. Meervelt, K. Binnemans, Chem. Commun. (2005) 590.
[15] B.D. Chandler, D.T. Cramb, G.K.H. Shimizu, J. Am. Chem. Soc. 128 (2006) 10403.
[16] J.-L. Song, J.-G. Mao, Chem. Eur. J. 11 (2005) 1417.
[17] X. Guo, G. Zhu, Q. Fang, M. Xue, G. Tian, J. Sun, X. Li, S. Qiu, Inorg. Chem. 44 (2005) 3850.
[18] X.D. Zhu, J. Lü, X.J. Li, S.Y. Gao, G.L. Li, F.X. Xiao, R. Cao, Cryst. Growth Des. 8 (2008) 1897–1901.
[19] X.M. Chen, M.L. Tong, Acc. Chem. Res. 40 (2007) 162–170.
[20] X.-M. Zhang, Coord. Chem. Rev. 249 (2005) 1201–1219.
[21] W.B. Lin, O.R. Evans, R.G. Xiong, Z.Y. Wang, J. Am. Chem. Soc. 120 (1998) 13272.
[22] C.M. Liu, S. Gao, H.Z. Kou, Chem. Commun. (2001) 1670.
[23] O.R. Evans, W.B. Lin, Acc. Chem. Res. 35 (2002) 511.
[24] X.M. Zhang, M.L. Tong, X.M. Chen, Angew. Chem. Int. Ed. 41 (2002) 1029.
[25] J. Tao, Y. Zhang, M.L. Tong, X.M. Chen, T. Yuen, C.L. Lin, X.Y. Huang, J. Li, Chem. Commun. (2002) 1342.
[26] R.H. Wang, M.C. Hong, J.H. Luo, R. Cao, J.B. Weng, Chem. Commun. (2003) 1018.
[27] CrystalClear, Version 1.35, Software User's Guide for the Rigaku R-axis and Mercury and Jupiter CCD Automated X-ray Imaging System, Rigaku Molecular Structure Corporation, The Woodlands, TX, USA, 2002.
[28] SHELXTL Reference Manual, Version 5.10, Siemens Analytical X-ray Instruments Inc., Madison, WI, USA, 1994.
[29] J.R. Li, X.H. Bu, R.H. Zhang, C.Y. Duan, M.C.K. Wong, V.W.W. Yam, New J. Chem. 28 (2004) 261.
[30] X.-H. Bu, W. Weng, M. Du, W. Chen, J.-R. Li, R.-H. Zhang, L.-J. Zhao, Inorg. Chem. 41 (2002) 1007.
[31] H. Bußkamp, G.B. Deacon, M. Hilder, P.C. Junk, U.H. Kynast, W.W. Lee, D.R. Turner, Cryst. Eng. Comm. 9 (2007) 394–411.
[32] C. Qin, X.L. Wang, E.B. Wang, L. Xu, Inorg. Chim. Acta 359 (2006) 417–423.
[33] D. Ang, G.B. Deacon, P.C. Junk, D.R. Turner, Polyhedron 26 (2007) 385–391.
[34] W.J. Evans, C.A. Seibel, J.W. Ziller, Inorg. Chem. 37 (1998) 770–776.
[35] J.Y. Lu, A.M. Babb, Inorg. Chem. 41 (2002) 1339–1341.
[36] X. Li, R. Cao, D. Sun, Q. Shi, W. Bi, M. Hong, Inorg. Chem. Commun. 6 (2003) 815–818.
[37] B. Li, W. Gu, L.-Z. Zhang, J. Qu, Z.-P. Ma, X. Liu, D.-Z. Liao, Inorg. Chem. 45 (2006) 10425–10427.
[38] J.-W. Cheng, S.-T. Zheng, G.-Y. Yang, Dalton Trans. (2007) 4059–4066.
[39] D.-W. Min, S.-W. Lee, Inorg. Chem. Commun. 5 (2002) 978–983.
[40] J.Y. Lu, J. Macias, J.G. Lu, J.E. Cmaidalka, Cryst. Growth Des. 2 (2002) 485–487.
[41] X.-W. Wang, X. Li, J.-Z. Chen, G. Zheng, H.-L. Hong, Eur. J. Inorg. Chem. (2008) 98–105.
[42] W. Chen, H.-M. Yuan, J.-Y. Wang, Z.-Y. Liu, J.-J. Xu, M. Yang, J.-S. Chen, J. Am. Chem. Soc. 125 (2003) 9266–9267.
[43] Z.-B. Han, X.-N. Cheng, X.-F. Li, X.-M. Chen, Z. Anorg. Allg. Chem. 631 (2005) 937–942.
[44] M. Li, J. Xiang, L. Yuan, S. Wu, S. Chen, J. Sun, Cryst. Growth Des. 6 (2006) 2036–2040.
[45] W.-P. Wu, Y.-Y. Wang, Y.-P. Wu, J.-Q. Liu, X.-R. Zeng, Q.-Z. Shi, S.-M. Peng, Cryst. Eng. Comm. 9 (2007) 753–757.
[46] G. Vicentini, L.B. Zinner, J. Zukerman-Schpector, K. Zinner, Coord. Chem. Rev. 196 (2000) 353.
[47] Y.J. Kim, M. Suh, D.Y. Jung, Inorg. Chem. 43 (2004) 245.

[48] Z.-H. Zhang, Y. Song, T. Okamura, Y. Hasegawa, W.-Y. Sun, N. Ueyama, Inorg. Chem. 45 (2006) 2896.
[49] Y.-G. Huang, B.-L. Wu, D.-Q. Yuan, Y.-Q. Xu, F.-L. Jiang, M.-C. Hong, Inorg. Chem. 46 (2007) 1171.
[50] X.L. Wang, C. Qin, E.B. Wang, Y.G. Li, N. Hao, C.W. Hu, L. Xu, Inorg. Chem. 43 (2004) 1850–1856.
[51] X.D. Zhu, X.J. Li, Q.Y. Liu, J. Lü, Z.G. Guo, J.R. He, R. Cao, J. Solid State Chem. 180 (2007) 2386–2392.